

Fractional-order Savitzky–Golay filter for pre-treatment of on-line Vis–NIR spectra to predict phosphorus in soil

Jian Zhang, Abdul M. Mouazen*

Department of Environment, Ghent University, Coupure Links 653, 9000 Gent, Belgium

*Corresponding author. Email: Abdul.Mouazen@UGent.be

Abstract

Visible and near infrared spectroscopy (vis-NIRS) has shown potential to predict soil phosphorous (P) with reasonable accuracy. However, spectra pre-treatment is essential in chemometric modelling. One of the most popular algorithms for spectral smoothing and differentiation is the integer-order Savitzky–Golay filter (IOSGF), which operates on a localised linear regression of several neighbouring points over a moving window. Herein, a modified Riemann–Liouville (RL) fractional-order Savitzky–Golay filter (MRLFOSGF) is presented based on the RL operators, as an extension of the conventional IOSGF. This filter was quantitatively analysed using power functions and Gaussian-type bands and were subsequently used to establish a partial least squares regression (PLSR) model for predicting P in soil. The results revealed that the MRLFOSGF offers significant flexibility with transition dynamics between integer-order SG derivatives and reduces baseline offsets and tilts. The PLSR model using the MRLFOSGF had a higher prediction accuracy than the corresponding PLSR model using the conventional IOSGF. This work demonstrates that the MRLFOSGF offers the advantage of wider applicability and better performance for predicting soil P than the conventional IOSGF.

Keywords: online vis-NIR spectroscopy; spectral pretreatments; soil phosphorous; fractional order calculus; Savitzky–Golay filter

1. Introduction

Nitrogen (N), phosphorus (P) and potassium (K) are three of the most essential nutrients for cereal crops production. They do not only significantly determine the growth rate of crops and thereby their final grain yield, but their relative contribution to grain dry matter also significantly determines grain quality. Despite being of a depletion source, P has accumulated in soils because of several decades of fertilising agricultural lands with larger doses of mineral P fertilisers or manure than the crops require, particularly in regions with intensive livestock production [1]. Although adding P to soils has

a positive impact on crop production, it has a negative impact on the environment. The accumulation of P in soils increases its potential to be in a soluble form, making it prone to losses via leaching and runoff, particularly in top soils with high P surpluses. This causes environmental pollution such as the eutrophication of freshwaters and algal bloom, which causes hypoxia and results in the deterioration of the water quality of fisheries and public health [2]. Therefore, knowledge of the soil P stock and budget in fields can help increase the efficiency of mineral fertilisers and manure while preventing environmental risks.

Soil P fractions can be measured with different laboratory methods. Traditionally, the extractable P (hereafter referred to as P) content in soils can be measured chemically by employing the Egner–Riehm–Domingo method to extract P with acid ammonium lactate (P-AL) at pH 3.75 in a laboratory. Although this wet chemical method is highly accurate, it is relatively expensive and time-consuming, requires an experienced technical expert and exposes chemicals into the environment. These shortcomings associated with the laboratory methods of chemical analyses in general prevent the analyses on large number of samples necessary for precision agricultural related variable rate applications. Therefore, innovative in situ soil sensors have been developed using advanced spectral technologies to achieve rapid, quantitative and non-invasive measurements. Visible–near-infrared (vis–NIR) spectroscopy is one of the most adopted spectral techniques for in situ soil scanning because it is fast, cost-effective and robust and allows for the quantification of several key soil fertility attributes, simultaneously [3-5]. Its sampling scale is very fine (e.g. >500 samples per ha), which enables precision agricultural solutions, e.g., variable rate (VR) fertilisation [6], VR manure application [7] and VR seeding [8], few to mention among others. However, multivariate calibration models are crucial for constructing calibration models that can predict the target soil properties from spectroscopic signals accurately. The workflow for generating the calibration consists of spectral pre-treatment and multivariate regression analyses, followed by independent validation of the resulting models. The objective of spectra pre-treatment is to enhance multivariable regression by removing sources of uninformative variance from the raw spectrum, hence, improve the prediction accuracy of the target soil property. This step is important for soil properties having indirect spectral responses in the NIR range, e.g., P, as prediction is attributed to covariation P has with other soil properties having direct spectral responses in NIR, e.g., moisture, mineralogy, and organic carbon [3], [9].

The most widely used pre-treatment methods in vis–NIR spectroscopy (in both reflectance and transmittance modes) can be classified into two categories: scatter correction methods and spectral derivatives [10]. The first group includes multiplicative scatter correction, standard normal variate and normalisation. There are three typical techniques for estimating spectral derivatives: finite differences, Savitzky-Golay (SG) filters and Norris–Williams (NW) derivatives. Despite the finite

differences are the simplest to calculate because they use the difference between adjacent points as the first-order derivative, they are not frequently used in practice because of noise inflation. The NW derivatives apply a moving average (MA) over the original data and calculate a finite difference after a previous smoothing step. Although the NW derivatives may provide similar estimates to SG filters, the latter is more frequently used because they were reported to provide better results [10]. The SG filter operates based on a local least-squares polynomial approximation to a specific set of input pixels in a symmetric window. It results in SG smoothing when the derivative order is set as zero and produces an integer-order derivative by performing differentiation on the fitted polynomial [11]. In particular, MAs are popular pre-treatment tools that are mathematically identical to SG smoothing with zero-degree polynomials (constant functions). Traditionally, SG filters are of integer orders (e.g., zero, first, and second orders). From a frequency domain perspective, SG filters can be regarded as a combination of a low-pass filter and an ideal derivative filter. They can be used to reduce high-frequency noise in spectra because of their smoothing feature (zero order) and reduce low-frequency signals using differentiation (non-zero integer order), thereby improving the contrast of relevant spectral features.

Non-integer-order differentiation, also known as a fractional-order derivative (FOD), is a generalisation wherein integer-order derivatives are only a subset of fractional orders that allow significant flexibility. Although there are numerous calculi related to non-integer orders, there is still no global consensus for their mathematical definition. The widely applicable fractional calculus can be mainly incorporated into the definitions of Riemann–Liouville (RL), Caputo and Grunwald–Letnikov (GL). Among all FOD definitions, the RLFOD is the most important and basic extension of ordinary differential calculi. Almost all other FOD definitions represent a special case of the RLFOD [12]. The Caputo FOD reformulates the RLFOD definition by exchanging the order of the ordinary derivative with the fractional integral. A common discretisation version known as the GL operator provides the most straightforward definition by constructing a finite difference similar to that of the NW derivative. However, additional parameters such as step size and memory length must be set in advance. Since the GL formula is one of the simplest FOD calculi, several studies have evaluated its potential in vis–NIR spectral pre-treatment by employing a GLFOD to directly process the entire spectrum [13]–[16]. It is not an SG-type filter because its filtering configuration does not require a moving window across the spectrum. An RL fractional-order SG filter has also been proposed for the treatment of noisy signals [17] and vis–NIR spectra [18]. However, such a filter would cause a counter-intuitive result in that the derivative of the constant term in polynomials would be non-zero when the derivative order is greater than 1. In light of this, we developed a modified RL fractional-order SG filter (MRLFOSGF) and evaluated its potential for improving the accuracy of P prediction in manure [19]. To the best of our knowledge, there is no study in the literature that explored the

potential application of any fractional-order SG filter (FOSGF) on on-line collected Vis–NIR soil spectra to improve the prediction of soil P.

The aim of this work is to evaluate the influence of MRLFOSGF in pre-treating on-line collected vis-NIR spectra for improving the prediction accuracy of soil P using partial least squares regression (PLSR), in comparison with the conventional IOSGF based PLSR model. In this study, a mathematical analysis was performed to demonstrate why MRLFOSGF can improve the performance of conventional IOSGF in spectral pre-treatment. Then, the influence of MRLFOSGF on accuracy of P prediction using PLSR is evaluated.

2. Materials and methods

2.1 Modified RL fractional order SG filter

In this section, the mathematical description of modified RL fraction order SG filter is introduced. An α^{th} -order RLFOD of a power function x^p ($p \geq 0$) is calculated as follows [17]:

$${}^{RL}D_x^\alpha(x^p) = \frac{\Gamma(p+1)}{\Gamma(p+1-\alpha)}x^{p-\alpha}, \quad (1)$$

where $\Gamma(z) = \int_0^\infty v^{z-1}e^{-v}dv$ is a gamma function.

A d^{th} -order (d is an integer) SG filter using an n -degree polynomial to fit the $2k+1$ point in the j window can be represented using the following formula:

$$\widehat{Y}_j^d = M_d(B^T B)^{-1}B^T Y_j, \quad (2)$$

where $B = \begin{bmatrix} 1 & 1 & \cdots & 1 \\ 1 & 2 & \cdots & 2^n \\ \vdots & \vdots & \ddots & \vdots \\ 1 & (2k+1) & \cdots & (2k+1)^n \end{bmatrix}$, \widehat{y}_j^d in $\widehat{Y}_j^d = [\cdots, \widehat{y}_j^d, \cdots]^T$ is the estimated d^{th} -order ($d \geq 0$)

differential value at point j , and M_d is denoted as

$$M_d = \begin{bmatrix} \overbrace{0, \cdots, 0}^{d \text{ columns}}, \cdots, & \frac{\Gamma(i)}{\Gamma(i-d)}, & \cdots, & \frac{\Gamma(n+1)}{\Gamma(n-d+1)} \\ 0, \cdots, 0, \cdots, & \frac{\Gamma(i)}{\Gamma(i-d)} 2^{i-1-d}, & \cdots, & \frac{\Gamma(n+1)}{\Gamma(n-d+1)} 2^{n-d} \\ \vdots & \vdots & \ddots & \vdots \\ 0, \cdots, 0, \cdots, & \frac{\Gamma(i)}{\Gamma(i-d)} (2k+1)^{i-1-d}, & \cdots, & \frac{\Gamma(n+1)}{\Gamma(n-d+1)} (2k+1)^{n-d} \end{bmatrix} \quad d+1 \leq i \leq n+1. \quad (3)$$

By combining the definition of the RL calculus presented in formula (1) with formulas (2) and (3), the MRLFOSGF is obtained using the following formula:

$$\widehat{Y}_j^\alpha = M_\alpha (B^T B)^{-1} B^T Y_j, \quad (4)$$

where \widehat{y}_j^α in $\widehat{Y}_j^\alpha = [\dots, \widehat{y}_j^\alpha, \dots]^T$ is the estimated α^{th} -order SG differential value at point j , and $M_\alpha^{\text{MRLFOSGF}}$ is an $(2k + 1) \times (n + 1)$ parameter matrix written as follows:

$$M_\alpha^{\text{MRLFOSGF}} = \begin{bmatrix} \overbrace{0, \dots, 0, \dots}^{[\alpha] \text{ columns}}, & \frac{\Gamma(i)}{\Gamma(i-\alpha)}, & \dots, & \frac{\Gamma(n+1)}{\Gamma(n+1-\alpha)} \\ 0, \dots, 0, \dots, & \frac{\Gamma(i)}{\Gamma(i-\alpha)} \cdot 2^{i-1-\alpha}, & \dots, & \frac{\Gamma(n+1)}{\Gamma(n+1-\alpha)} \cdot 2^{n-\alpha} \\ \vdots & \vdots & \vdots & \vdots \\ 0, \dots, 0, \dots, & \frac{\Gamma(i)}{\Gamma(i-\alpha)} \cdot (2k+1)^{i-1-\alpha}, & \dots, & \frac{\Gamma(n+1)}{\Gamma(n+1-\alpha)} \cdot (2k+1)^{n-\alpha} \end{bmatrix} \quad [\alpha] + 1 \leq i \leq n + 1, \quad (5)$$

where $[\cdot]$ denotes the rounding down to the next lower integer of α .

Since the RLFOD exhibits a feature, in which FOD (α is not an integer) of a constant is non-zero, it results in a counter-intuitive result wherein the α^{th} derivative of the constant term in a fitted polynomial is non-zero when $\alpha > 1$. MRLFOSGF using formula (5) would have zero values in the first column corresponding to the constant terms in an polynomial if the derivative order is greater than 1. Similarly, when using a non-integer-order derivative that is larger than the second order, both the constant and first term of the fitted polynomial would be zero since the first two columns of $M_\alpha^{\text{MRLFOSGF}}$ are zero. This is intuitively consistent with integer-order derivatives.

On the other hand, since $\frac{\Gamma(i)}{\Gamma(i-\alpha)} \cdot (2k+1)^{i-1-\alpha} = \frac{\Gamma(i)}{\Gamma(i-d)} (2k+1)^{i-1-d}$ when $\alpha = d$, the formula (5) covers the conventional IOSGFs in formula (3), such as the SG smoothing filter ($\alpha = d = 0$), the first-order SG derivative ($\alpha = d = 1$) and the second-order SG derivative ($\alpha = d = 2$). This means that the integer orders can be considered special cases of formulas (4) and (5) when α is of an integer order. Formulas (4)-(5) were incorporated into a code package developed for implementing MRLFOSGF using MATLAB.

2.2 On-line Vis-NIR spectra acquisition

A multi-sensor platform developed by Mouazen (2006) was used to collect on-line vis-NIR spectra of soils (Fig. 1) [20]. The platform is equipped with a subsoiler that penetrates the soil, creating a ditch with a depth range of 15–25 cm. The soil spectra were collected in the reflectance mode using

an optical probe connected to a vis–NIR sensor (tec5 AG, Germany) with a measurement range of 305–1700 nm. A 100% ceramic disc was used as the white reference to correct the on-line soil spectra every 30 min. A differential global positioning system (DGPS, CFX-750, Trimble, USA) with a data logger (Compact Rio 9082, National Instruments, USA) was used to synchronically log and record DGPS positions and reflectance spectra at a frequency of 1 Hz. This was done using multi-sensor data logging and acquisition software developed using the LabVIEW programming environment. During the field scan, the platform was driven by a tractor along parallel scanning transects (12 m apart) at an average travel speed of about 3.6 km/h.

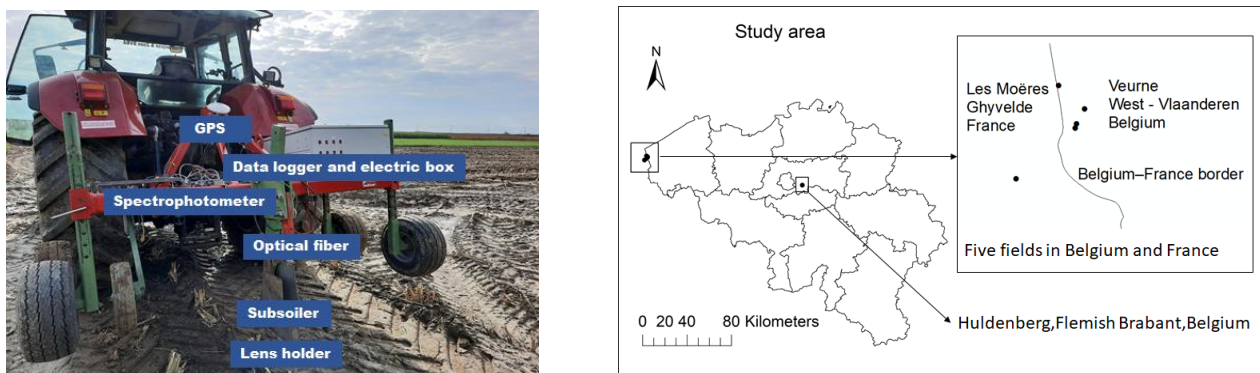


Fig. 1. Multiple-sensor platform used for on-line sensing of soil spectra using visible and near infrared spectroscopy (vis-NIRS) of Mouazen (2006) and study area

On-line measurements were conducted after harvesting of previous crops on six fields in Belgium and France between 2018 and 2020. Altogether, 165 samples were randomly collected from the smooth bottom of the trench formed by the subsoiler during the on-line measurement. Each soil sample was mixed well and cleaned by removing plant residues, stones or roots in the laboratory. The samples were then reduced to sub-samples of 150 g using the quartering method. These sub-samples were subjected to chemical analysis using the traditional laboratory methods of the Soil Survey of Belgium (BDB, Heverlee, Belgium). The extractable P content in the soil was measured by extracting P using ammonium lactate at a pH of 3.75 using the Egner–Riehm–Domingo method [21].

2.3 Spectral pre-treatment and soil P modelling

The on-line collected spectra were subjected to several pre-treatment steps before the calibration-validation stage. First, the vis–NIR spectra were pre-treated by removing the spectral jump at 1045 nm, where the two vis and NIR detectors join. Thereafter, the noisy parts of the spectra at the two ends were removed. Then, the neighbouring wavelengths were averaged using the MA algorithm (SG smoothing with the zero-degree polynomial), followed by normalisation to a range of –1 to 1. Spectra derivatives were calculated using the MRLFOSGF and IOSGF respectively, which was followed by

SG smoothing. The window size of the MA and the normalisation range were set to the same values when comparing the performances of the MRLFOSGF and IOSGF.

PLSR cross-validation and independent validation were performed by dividing the entire dataset into calibration (70%) and validation (30%) sets. PLSR was performed on the calibration set using a leave-one-out cross-validation method to develop the calibration model. The developed calibration models were validated using the independent validation set. The prediction performance of the developed models was evaluated using the coefficient of determination (R^2), root mean square error (RMSE), ratio of performance to inter-quartile distance (RPIQ) and residual prediction deviation (RPD).

3. Results and discussion

3.1 Effects of MRLFOSGF on polynomial fitting

SG derivatives are the differentiation of a least-squares polynomial used for SG smoothing to fit an array x of $2k + 1$ points $x_1 \cdots x_{2k+1}$ to the sum of several power functions over a moving window:

$$f(x) = c_0 + c_1x^1 + \cdots c_nx^n = \sum_{p=0}^n c_p x^p \quad (6)$$

Since the first-order and second-order SG derivatives of quadratic and cubic polynomials are commonly used in the literature, the effects of fractional-order SG derivatives on polynomial fitting are evaluated when the polynomial order $n = 3$. Table 1 shows the FODs of power functions that can be calculated analytically from the zeroth to second order using formula (1).

Table 1. Examples of zero- to second- order modified Riemann–Liouville (RL) fractional-order Savitzky–Golay filter (MRLFOSGFs) of zero- to three- degree power functions, and different filter order α

	x^0	x^1	x^2	x^3
$\alpha = 0.2$	$\frac{1}{\Gamma(0.8)}x^{-0.2}$	$\frac{\Gamma(2)}{\Gamma(1.8)}x^{0.8}$	$\frac{\Gamma(3)}{\Gamma(2.8)}x^{1.8}$	$\frac{\Gamma(4)}{\Gamma(3.8)}x^{2.8}$
$\alpha = 0.4$	$\frac{1}{\Gamma(0.6)}x^{-0.4}$	$\frac{\Gamma(2)}{\Gamma(1.6)}x^{0.6}$	$\frac{\Gamma(3)}{\Gamma(2.6)}x^{1.6}$	$\frac{\Gamma(4)}{\Gamma(3.6)}x^{2.6}$
$\alpha = 0.6$	$\frac{1}{\Gamma(0.4)}x^{-0.6}$	$\frac{\Gamma(2)}{\Gamma(1.4)}x^{0.4}$	$\frac{\Gamma(3)}{\Gamma(2.4)}x^{1.4}$	$\frac{\Gamma(4)}{\Gamma(3.4)}x^{2.4}$
$\alpha = 0.8$	$\frac{1}{\Gamma(0.2)}x^{-0.8}$	$\frac{\Gamma(2)}{\Gamma(1.2)}x^{0.2}$	$\frac{\Gamma(3)}{\Gamma(2.2)}x^{1.2}$	$\frac{\Gamma(4)}{\Gamma(3.2)}x^{2.2}$
$\alpha = 1$	0	1	$2x$	$3x^2$
$\alpha = 1.2$	0	$\frac{\Gamma(2)}{\Gamma(0.8)}x^{-0.2}$	$\frac{\Gamma(3)}{\Gamma(1.8)}x^{0.8}$	$\frac{\Gamma(4)}{\Gamma(2.8)}x^{1.8}$
$\alpha = 1.4$	0	$\frac{\Gamma(2)}{\Gamma(0.6)}x^{-0.4}$	$\frac{\Gamma(3)}{\Gamma(1.6)}x^{0.6}$	$\frac{\Gamma(4)}{\Gamma(2.6)}x^{1.6}$
$\alpha = 1.6$	0	$\frac{\Gamma(2)}{\Gamma(0.4)}x^{-0.6}$	$\frac{\Gamma(3)}{\Gamma(1.4)}x^{0.4}$	$\frac{\Gamma(4)}{\Gamma(2.4)}x^{1.4}$
$\alpha = 1.8$	0	$\frac{\Gamma(2)}{\Gamma(0.2)}x^{-0.8}$	$\frac{\Gamma(3)}{\Gamma(1.2)}x^{0.2}$	$\frac{\Gamma(4)}{\Gamma(2.2)}x^{1.2}$
$\alpha = 2$	0	0	2	$6x$

Since the MRLFOSGF is a linear operator, i.e.

$${}^{RL}D_x^\alpha (\lambda f(x) + \gamma g(x)) = \lambda ({}^{RL}D_x^\alpha f(x)) + \gamma ({}^{RL}D_x^\alpha g(x)), \quad (7)$$

the fractional-order SG derivatives of a fitted polynomial can be written as a linear combination of the derivatives of the power functions listed in Table 1. Figure 2 illustrates the behaviour of fractional-order SG derivatives of power functions over a moving window of size 9 based on the information presented in Table 1.

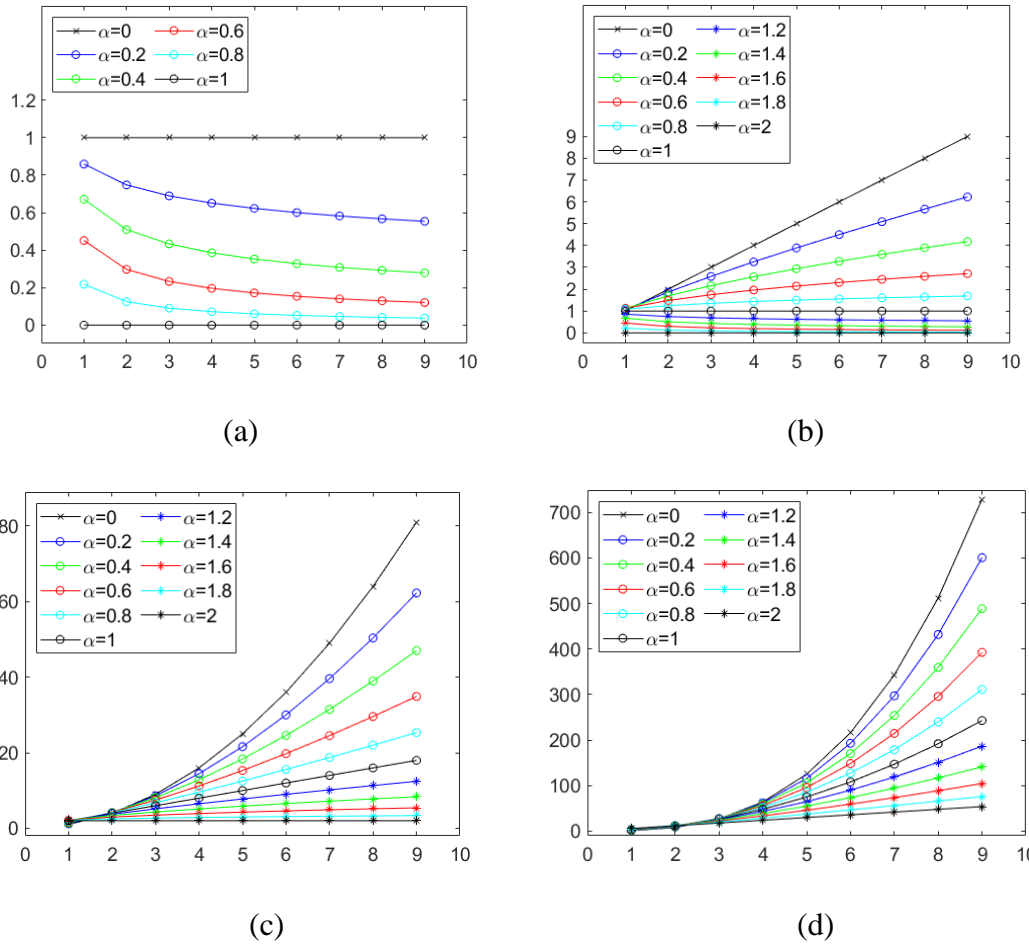


Fig. 2. Fractional-order Savitzky–Golay (SG) derivatives of different power functions x^0 , x^1 , x^2 and x^3 and different filter order α

When the order increases by 0.2, the MRLFOSGF exhibits the ‘interpolation’ characteristic, which is one of the main points for understanding why FODs provide more flexible outcomes than the IODs. Even for constant terms, decimal derivatives have transition behaviours between the first order and the zero order derivatives. Since the derivative curves are continuously transitioned with respect to the order of derivatives, both 0.8th-order and 1.8th-order derivatives exhibit more similarity to the first-order and second-order derivatives, respectively, for the power functions $p = 1, 2, 3$. Although the second-order SG derivative can eliminate a sloping baseline and enhance spectral resolution, it amplifies undesired noise and corrupt spectral signals when compared to the first-order SG derivative. Therefore, working with a practical spectrum requires a compromise between the benefits of the different orders of SG filters. However, the conventional IOSGF used in NIR spectral pre-treatment has almost only a few options, such as first or second order, whereas the MRLFOSGF offers much more options.

Curve fitting techniques are invaluable resources for approximating NIR spectra because they sometimes allow for both the mathematical description of band shapes and the qualitative and quantitative estimations of absorption components [22]. It implies that the absorption bands, when analysed as log reflectance versus photon energy (wavelength), can be fitted numerically to illustrate the basic features using Gaussian, modified Gaussian, Lorentz or combined Gaussian–Lorentz (Voigt) functions [23]-[24]. To evaluate the potential of MRLFOSGF, simulated reflectance bands with shoulder peaks were generated by employing the 10-based exponential function of negative absorbance expressed as follows:

$$R = 10^{-A}, \quad (8)$$

where the absorbance bands with a shoulder peak and white noise were derived from the following analytical function, which represents the Gaussian-type profile on a sloping baseline:

$$A(\omega) = h \cdot \left(\frac{\omega}{\omega_0}\right)^m \cdot \left(e^{-\frac{(\omega-\omega_0)^2}{\sigma^2}} + 0.05 e^{-\frac{(\omega-\omega_s)^2}{\sigma_s^2}} + D \right), \quad (9)$$

where h denotes the band strength, ω_0 and ω_s are the centres of the major and shoulder peaks, respectively, σ and σ_s are the widths of both peaks, and m and D are the power-law slope and constant offset of the baseline, respectively. The function $\left(\frac{\omega}{\omega_0}\right)^m$ was used to represent the wavelength dependence of the baseline stems from owing to the observation that the spectral baselines of a wide variety of particulate media can be fitted well by power curve [25].

Figure 3(a) depicts the simulated spectra based on formulas (8) and (9) in the range of 1250–1650 nm without (red curve) and with (blue curve) noise. It can be observed that the major dip occurs at 1450 nm, whereas a small shoulder dip occurs at 1550 nm. Since white noise is present in almost all analytical measurements and is often attributed to the photometric noise in detection instruments, white noise equal to 1% of the noisy signal in terms of root mean square (RMS) was added to investigate the benefits of the MRLFOSGF.

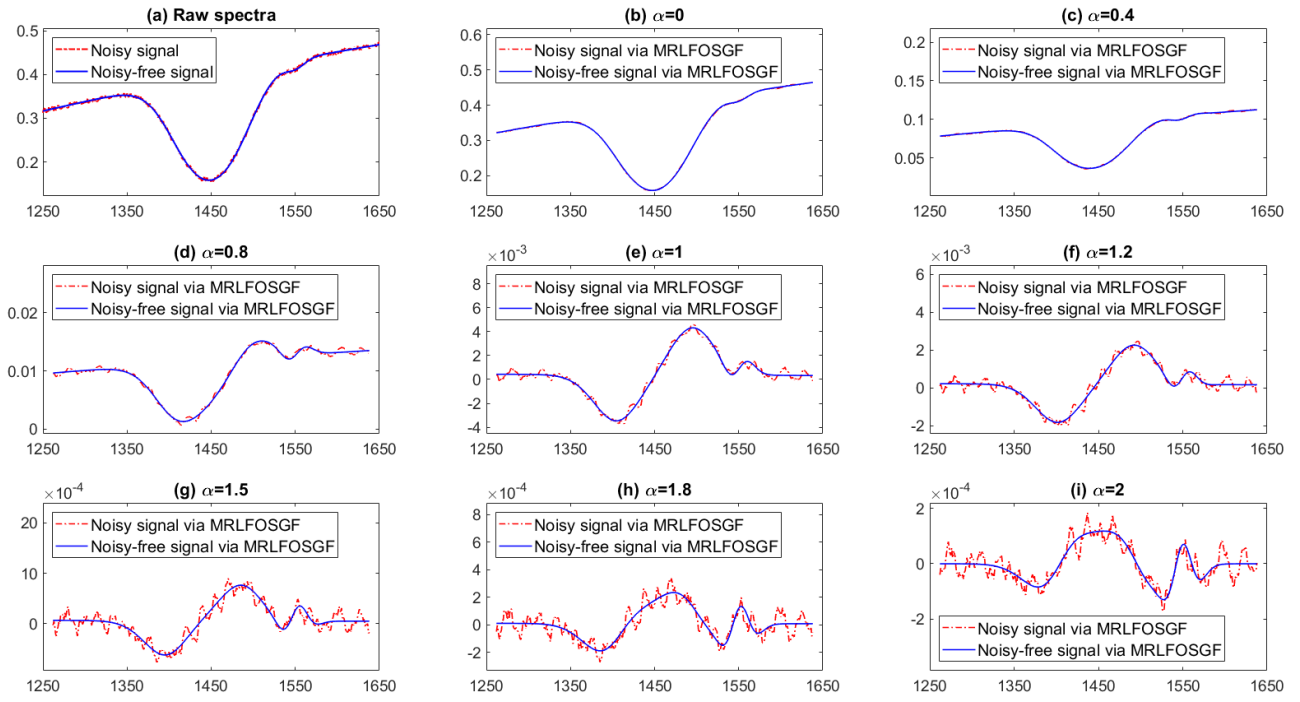


Figure 3. Simulated reflectance bands with both major and shoulder dips after applying modified Riemann–Liouville (RL) fractional-order Savitzky–Golay filter (MRLFOSGF), shown for different filter order α

The developed program can be used to calculate the different orders of derivative under a moving window size of 25 with a fitting cubic polynomial. Figures 3(b)–(i) depict typical curves for $0 \leq \alpha \leq 2$. The conventional SG filter and MRLFOSGF coincide with each other at integer orders ($\alpha = 0, 1$ and 2). The MRLFOSGF smoothly and gradually transforms the differentiated major noise-free dip at 1450 nm from its original shape (Fig. 3 [b]) into a bipolar shape at $\alpha = 1$ (Fig. 3 [g]) and finally into a peak with two smaller side lobes at $\alpha = 2$ [Fig. 3 (i)]. Moreover, the small shoulder dip at 1550 nm can be observed when the derivative order increases from 0.8 [Fig. 3 (d)] to 2 [Fig. 3 (i)], and it increases in size as the derivative order increases until it transforms into an evident peak and a sharp peak in the first-order and second-order derivative spectra, respectively. These results demonstrate that the MRLFOSGF can interpolate between IODs, as described in Table 1. Figure 3 also shows that the offset and slope of the baseline progressively diminish as the α^{th} order of the FOD increases from 0 to 2. They are all approximately reduced to 0 when $\alpha = 2$.

Although the second-order derivative can better identify the shoulder dip in Fig. 3 (a) than the first-order derivative, it greatly amplifies the white noise involved in the spectrum. As shown in Table 2, the variations in the noise-to-signal ratio (NSR) were calculated with respect to the derivative order to evaluate the performance of MRLFOSGF that can be offered to noisy spectra, where NSR is defined in terms of RMS, i.e. NSR is equal to the RMS of the noise divided by the RMS of the full

signal. It can be observed that the MRLFOSGF reduces the NSR of the noisy spectrum when α is in the range of 0 – 0.4, demonstrating more smoothing effects that are very similar to the effect of the SG smoothing filter ($\alpha = 0$). However, the derivative spectrum is almost drowned in the noise when $\alpha \geq 1.8$ to the extent that it is impossible to separate the useful information from the derivative results. Mathematically, this can be explained by the fact that the MRLFOSGF with high derivative orders amplifies noise when $\alpha > 1$. Therefore, smooth filtering should be conducted before using derivatives since noise will be inevitably produced by NIR instruments, the experimental environment and operational errors.

Table 2. NSR* calculated for different α^{th} -orders between 0 and 2

	α order								
	Raw	0	0.4	0.8	1	1.2	1.5	1.8	2
MRLFOSGF	1%	0.3%	0.7%	3%	13.7%	21.1%	35.7%	47.5%	46.8%

* NSR = (root mean square of noise after processing by MRLFOSGF) / (root mean square of full signal after processing by MRLFOSGF), MRLFOSGF is modified Riemann–Liouville (RL) fractional-order Savitzky–Golay filter.

3.2 Soil spectra variation with pre-treatments

Figures 4 (a) depict the on-line collected soil raw reflectance spectra. Figures 4 (b)–4 (i) present the derivative spectra at different α^{th} orders. Soils darken as their organic matter (OM) and moisture contents increase, resulting in an increase in absorbance and an equivalent decrease in their ability to reflect light. This is consistent with the spectral shape shown in Fig. 4 (a), whose reflection is low at the visible range due to the blue absorption band at 450 nm related to OM. The distinct reflectance valley at around 1450 nm is caused by the strong absorbance of radiation by water molecules of the fresh soils (Fig. 4), which is attributed to the second overtone of the fundamental vibration of the O–H molecule bond [26]. Weak bands located near 1130 nm are due to vibrations caused by the O–H and C–H bonds of free water as well as water present in the lattice of various clay minerals or water adsorbed on the particle surfaces [27]. Additionally, free water occupies soil pores with additional weak reflectance bands related to the stretching vibration of the O–H groups near 980 nm [28]. Soil OM is a mixture of dead plant and animal tissues as well as substances secreted by organic organisms during various degradation stages. Therefore, it is one of the most important properties of agricultural soils. The group of absorption bands at around 630 nm may be attributed to pigment residuals of plant debris, such as chlorophyll [29]. Only weak absorption features could be observed because chlorophyll pigments are thought to decompose rapidly with time. Other potential absorption at this

band is attributed to absorption of iron oxides, related to the red colour absorption band at 650 nm [30].

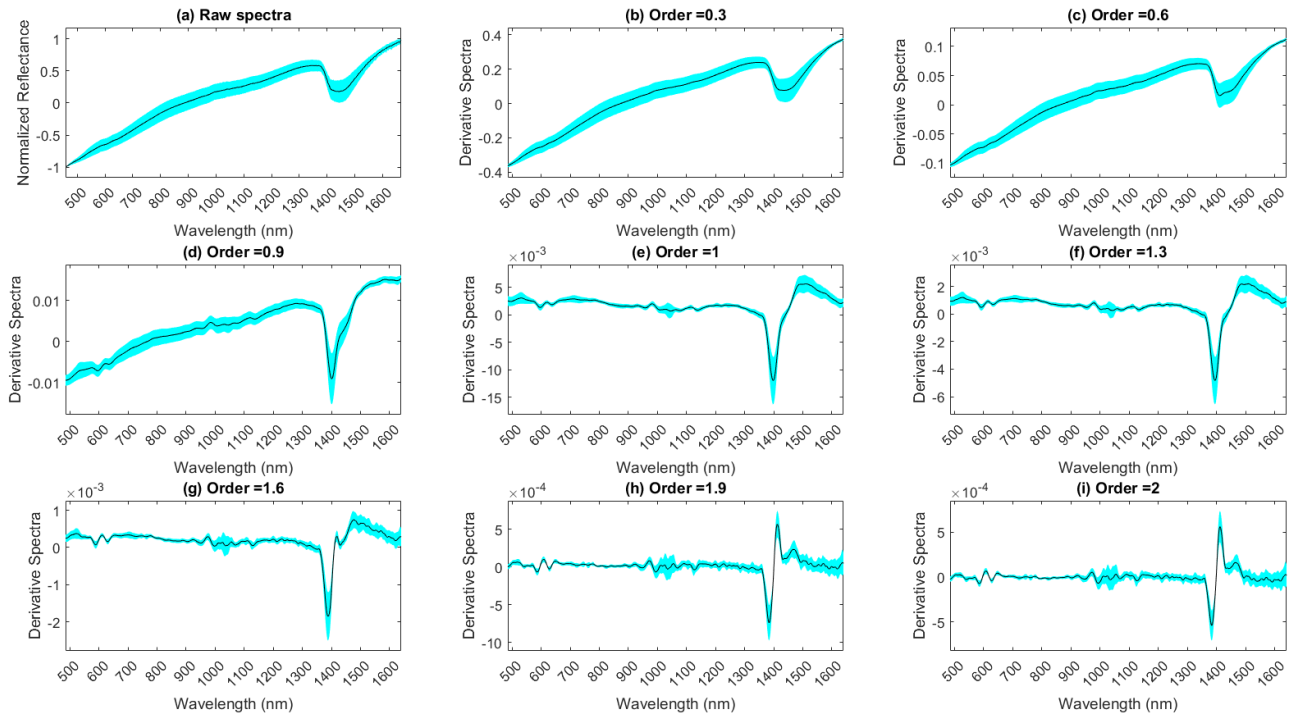


Fig. 4. Fractional-integer order derivative spectra of on-line spectra of 165 soil samples used in this study, shown for different derivative orders from 0.3 to 2. Cyan areas represent the standard deviations of the spectra and the black curves are the mean of spectra of the soil samples

The reflectance profiles made by the MRLFOSGF exhibited continuous variations when the derivative order increased from 0 to 2 (Fig. 4). The baseline offset effects gradually decreased as the derivative order increased. Although the 0.6th-order derivative sharpened the valleys and peaks, a relatively large offset and slope were observed; however, the magnitude of the high-frequency noise in the derivative spectrum remained low. The 0.9th-order derivative decreased the offset and slope substantially without increasing the noise effect. The peaks and valleys sharpened further as the order increased from 0.9 to 2. The features of the 1.9th-order derivative spectra were overwhelmed by the noise, and a few small peaks appeared, indicating that the higher-order derivative spectra were more susceptible to interferences from spectral noises. This observation is consistent with results presented in Figure 3 and Table 2, which indicate that the fractional order derivative spectra produced by MRLFOSGF can capture changes in spectral details and improve spectral curve resolution. However, an aggressive derivative with a high order of 1.8 or more must be used cautiously to prevent noise introduction. These results suggest that the MRLFOSGF derivative spectra have advantages over the conventional integer order derivative spectra because they allow users to optimise the performance of regression model by adjusting the derivative order with small intervals. Furthermore, the IOSGFs

can be considered as special cases of presented algorithm. Therefore, the performance of the proposed MRLFOSGF would not be worse than that of the conventional.

3.3 PLSR model prediction performance

After pre-treatment based on different derivative orders, PLSR models were developed to evaluate the influence of the MRLFOSGF on the prediction performance of the P model. Table 3 shows the prediction results indicated as R^2 , RMSE, RPD and RPIQ. Overall, the 1.3rd-order derivative spectral-based model by the MRLFOSGF outperformed the other models, with R^2 values of 0.75 and 0.70, which were an increase of 0.03 and 0.06 for the calibration and validation set, respectively, when compared to that of the first order. These results prove that the MRLFOSGF algorithm has a positive effect on model performance. The 1.6th-order derivative performed similarly to the first-order derivative for the validation set. Contrarily, the second-order derivative exhibited the worst prediction performance for the validation set.

Table 3 shows that there is no linear dependency or qualitative relationship between the derivative order and model performance. Increasing or decreasing the derivative order does not necessarily increase or decrease the model prediction performance, and this appears to be true for the same dataset. Perhaps it is dataset-specific, material-specific and parameter-specific, implying that an optimal derivative order may be dependent on the dataset itself. Since the MRLFOSGF algorithm can be implemented simply, order tuning can be optimised by repeated trial and error, and the best order can be chosen as the order that produces the largest R^2 , RPD and RPIQ values and the smallest RMSE values. It does not require detailed knowledge of the separate effects of interfering substances, background scattering or high-frequency noise. For example, the optimal order in this study was 1.3, but the optimal order may be 0.9, 1.2, 1.4 or other values in other application cases. This trend is similar to that of other pre-treatment algorithms, such as the MA. For highly variable datasets, a small window size of the MA may be crucial for increasing sensitivity to changes; contrarily, for noisy datasets, a large window size should be considered to decrease noise. However, there is also no theoretical argument that permits the determination or calculation of the optimal moving window width.

Table 3. Predictive results for phosphorous (P) estimation in soil using partial least squares regression (PLSR) established with eight derivative orders. Results are shown for calibration and validation sets.

Order	Calibration				Validation			
	R ²	RPD	RMSE (mg/100g)	RPIQ	R ²	RPD	RMSE (mg/100g)	RPIQ
0.3	0.54	1.48	5.84	1.63	0.36	1.27	5.87	1.58
0.6	0.58	1.55	5.55	1.71	0.40	1.31	5.69	1.63
0.9	0.66	1.72	5.01	1.90	0.50	1.42	5.22	1.77
1	0.72	1.89	4.56	2.08	0.64	1.67	4.45	2.08
1.3	0.75	2.02	4.27	2.23	0.70	1.84	4.04	2.28
1.6	0.81	2.31	3.74	2.54	0.64	1.70	4.38	2.11
1.9	0.80	2.26	3.82	2.49	0.45	1.36	5.45	1.70
2	0.79	2.17	3.98	2.39	0.39	1.29	5.76	1.61

Coefficient of determination (R²), root means square error (RMSE), ratio of performance to inter-quartile distance (RPIQ), and residual prediction deviation (RPD). Very poor: RPD < 1.0, Poor: RPD = 1.0-1.4, Fair: RPD = 1.4-1.8, Good: RPD = 1.8-2.0, Very good: RPD = 2.0-2.5, Excellent: RPD > 2.5, Very poor: RPIQ < 1.4, Fair: RPIQ = 1.4-1.7, Good: RPIQ = 1.7-2.0, Very good: RPIQ = 2.0-2.5, Excellent: RPIQ > 2.5.

Figure 5 shows the scatterplots of the measured P content in comparison to the P content predicted by the PLSR model based on the best performing 1.3rd-order derivative spectra. The points were grouped along the 1:1 line. This distribution indicates a linear relationship between the measured P and the predicted P. Compared to conventional first-order SG derivative spectra, the 1.3rd-order derivative spectra improved the model accuracy by (0.03, 0.13, 0.15) and (0.06, 0.17, 0.20), as measured by the R², RPD and RPIQ values for the calibration and validation sets. Therefore, the MRLFOSGF exhibits good potential in spectral pre-treatment for predicting P in soil under field conditions using on-line collected soil spectra.

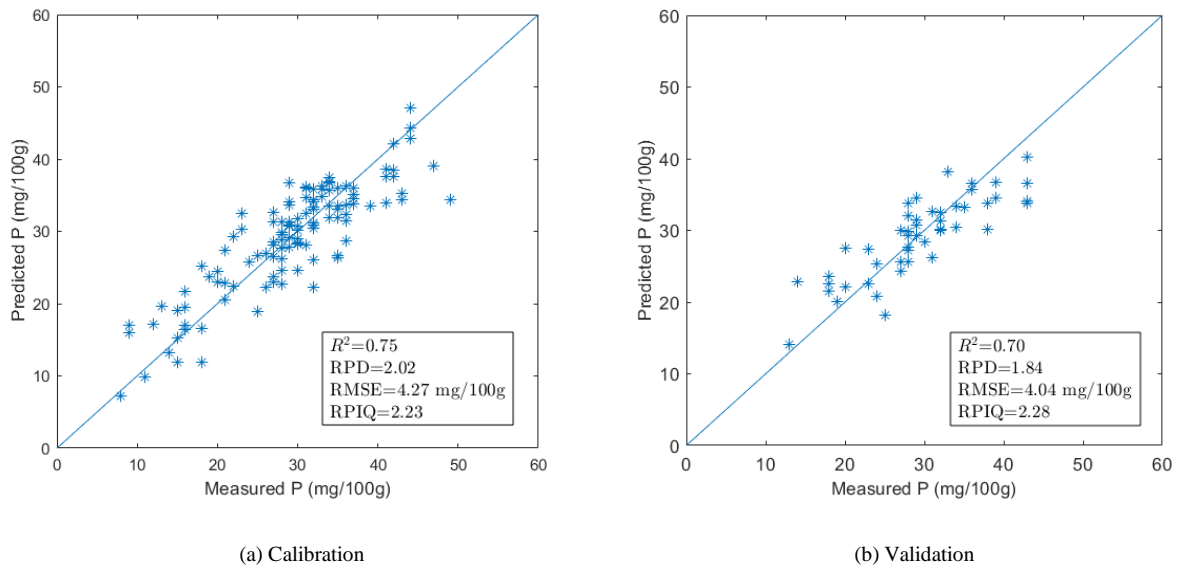


Fig. 5. Scatter plots of the measured phosphorous (P) content vs. P content predicted using the best performing 1.3-order derivative spectra-based partial least squares (PLSR) model

Mouazen et al. [31] stated that even though P in soil is not spectrally active in the NIR range, its successful prediction in the literature may be attributed to covariation with other properties that have direct spectral responses in the NIR spectrometry. The variation of vis–NIR spectra of soils are due to the radiation absorbed by various chemical bonds (e.g. C–H, N–H, O–H, C–O, C–N and N–O) in soil organic constituents, as well as Ca–O, Fe–O and Al–O in minerals [9]. P availability is directly affected by soil organic matter (OM) content, paedogenic oxides, carbonates and clay minerals. It depends on the relative loading of P onto the available reactive clay and paedogenic oxide surfaces; the soil pH, which partly depends on the CaCO₃ content; and the soil organic P content, which is a direct function of the soil OM content [32]. A vis–NIR spectroscopy has indeed been successfully used to predict these P-availability determinants including soil texture attributes, particularly the clay content, mineralogy, OM and moisture content. The estimates of these attributes have also been shown to be robust [3]. Moreover, NIR spectroscopy has frequently been used to accurately predict other soil attributes that are spectrally inactive in the NIR range, such as pH, potassium, manganese, zinc and copper. In light of these, successful prediction of P using NIR has been reported for fresh soil samples [33]. However, these same authors used soil spectra collected under laboratory conditions. Later, the same authors developed a PLSR calibration model for soil P prediction using on-line collected spectra from several fields in Belgium and Northern France, using the tradition SG spectra derivation [34]. The PLSR model provided accurate estimation of P but with a larger RMSE of 11.523 mg/100g, than that of the current work (4.04 mg/100g for the filter order of 1.3 [Table 3]. Mouazen et al. (2016) developed a calibration model for soil P using on-line collected spectra of 383

samples collected from several fields in the UK [35]. Despite the RMSE of 0.6 mg/100g was much smaller than the that of current work (Table 3), both RPD (1.5) and R^2 values of the prediction set (0.6) were also lower. These mixed accuracies reported so far, using the same on-line spectroscopy sensor [20] may well be attributed to the indirect response soil P has with soil attributes having direct spectral responses in the NIR spectral range. Despite the variable prediction accuracy the on-line system enables high sampling resolution data necessary for variable rate P fertilisation and manure application [36]. Thanks to the on-line vis-NIR sensing system enabling the collection of high quality soil spectra resulting in reasonable prediction accuracy for P over small distance intervals. The MRLFOSGF contributes to the accurate estimation of P, for improved site-specific management of manure and P fertilisers.

4. Conclusions

The MRLFOSGF is proposed for calculating FOSGF with an arbitrary order. The developed program was used to investigate the effects of FOSGF filters on vis-NIR spectral pre-treatment. The filters were further applied to on-line soil spectra before they were then used as input for PLSR modelling to estimate soil P. The results led to the following conclusions:

- 1) The MRLFOSGF offers better flexibility than conventional IOSGFs because it can interpolate the power functions between integer-order SG derivatives and decrease baseline offsets and tilts by finely adjusting the derivative order.
- 2) The MRLFOSGF produces a better model for predicting the P content in soil in terms of R^2 , RMSE, RPD and RPIQ than traditional first-order and second-order SG filters.
- 3) The differential order of MRLFOSGFs must be tuned through trial and error, and the best order can be selected as the order that provides the highest accuracy.

In future studies, the MRLFOSGF will be combined with other advanced pre-treatment algorithms and modelling methods, such as the weighted MA and nonlinear machine learning methods, to further improve the prediction of P in soils in a mathematically interpretable sense.

Acknowledgement

This research was funded by the Research Foundation—Flanders (FWO) for the Odysseus I SiTeMan Project (Nr. G0F9216N).

References

- [1] P. Panagos, J. Köningner, C. Ballabio, L. Liakos, A. Muntwyler, P. Borrelli, E. Lugato, Improving the phosphorus budget of European agricultural soils, *Science of the Total Environment*, 853 (2022) 158706.
- [2] E.R. Lucas, G.S. Toor, J.M. McGrath, Agronomic and environmental phosphorus decline in coastal plain soils after cessation of manure application, *Agriculture, Ecosystems & Environment*, 311 (2021) 107337.
- [3] B.Y. Kuang, H.S. Mahmood, M.Z. Quraishi, W.B Hoogmoed, A.M. Mouazen, E.J. van Henten, Sensing soil properties in the laboratory, in Situ, and on-Line: a review, *Advance in Agronomy*, 114 (2012) 155-223.
- [4] D. Xiao, J. Huang, J. Li, Y.H. Fu, Y.C. Mao, Z.N. Li, N.S. Bao, Inversion study of soil organic matter content based on reflectance spectroscopy and the improved hybrid extreme learning machine, *Infrared Physics & Technology*, 128 (2023) 104488.
- [5] A. Bahrami, M. Danesh, M. Bahrami, Studying sand component of soil texture using the spectroscopic method, *Infrared Physics & Technology*, 122 (2022) 104056.
- [6] A. Guerrero, S. De Neve, A.M. Mouazen, Data fusion approach for map-based variable-rate nitrogen fertilization in barley and wheat, *Soil & Tillage Research*, 205 (2021) 104789.
- [7] J. Zhang, A. Guerrero, A.M. Mouazen, Map-based variable-rate manure application in wheat using a data fusion approach, *Soil & Tillage Research*, 207 (2021) 104846.
- [8] M.A. Munnaf, A.M. Mouazen, Development of a soil fertility index using on-line Vis-NIR spectroscopy, *Computer and Electronic in Agriculture*, 188 (2021) 106341.
- [9] B. Stenberg, R.A. Viscarra Rossel, A.M. Mouazen, J. Wetterlind, Visible and near infrared spectroscopy in soil science, *Advances in Agronomy*, 107 (2010) 163-215.
- [10] Å. Rinnan, F. van Den Berg, S.B. Engelsen, Review of the most common pre-processing techniques for near-infrared spectra, *TrAC Trends in Analytical Chemistry*, 28 (10) (2009) 1201-1222.
- [11] R.W. Schafer, What is a Savitzky - Golay filter?, *IEEE Signal Processing Magazine*, 28(4) (2011) 111–117.
- [12] H.A. Fallahgoul, S.M. Focardi, F.J. Fabozzi, Fractional calculus and fractional processes with applications to financial economics: Theory and application, Academic Press 2016.

- [13] Y.S. Hong, Y.L. Liu, Y.Y. Chen, Y.F. Liu, L. Yu, Y. Liu, H. Cheng, Application of fractional-order derivative in the quantitative estimation of soil organic matter content through visible and near-infrared spectroscopy, *Geoderma*, 337 (2019) 758-769.
- [14] Y.S., Hong, L. Guo, S.C. Chen, M. Linderman, A.M., Mouazen, L. Yu, Y.Y. Chen, Y.L. Liu, Y.F. Liu, H. Cheng, Y. Liu, Exploring the potential of airborne hyperspectral image for estimating topsoil organic carbon: Effects of fractional-order derivative and optimal band combination algorithm, *Geoderma*, 365 (2020) 114228.
- [15] J. M. Schmitt, Fractional Derivative Analysis of Diffuse Reflectance Spectra. *Applied Spectroscopy*, 52(6) (1998) 840-846.
- [16] Y.S. Hong, S.C. Chen, Y.L. Liu, Y. Zhang, L. Yu, Y.Y. Chen, Y.F. Liu, H. Cheng, Y. Liu, Combination of fractional order derivative and memory-based learning algorithm to improve the estimation accuracy of soil organic matter by visible and near-infrared spectroscopy. *CATENA*, 174 (2019) 104-116.
- [17] D.L. Chen, Y.Q. Chen, D.Y. Xue, Digital fractional order Savitzky-Golay differentiator, *IEEE Transactions on Circuits and Systems II: Express Briefs*, 58 (11) (2011) 758-762.
- [18] P.J., Tong, Y.P. Du, K.Y. Zheng, T. Wu, J.J. Wang, Improvement of NIR model by fractional order Savitzky–Golay derivation (FOSGD) coupled with wavelength selection, *Chemometrics and Intelligent Laboratory Systems*, 143 (2015) 40-48.
- [19] J. Zhang, A. M. Mouazen, 2023. A novel non-integer order Savitzky–Golay derivative function of visible and near-infrared spectra for improving prediction accuracy of phosphorus in pig manure. (Under review).
- [20] A.M. Mouazen, Soil Survey Device, International Publication Published Under the Patent Cooperation Treaty (PCT), World Intellectual Property Organization. WO2006/015463, PCT/BE2005/000129, 2006.
- [21] K. Sardi, P. Csathó, Studies on the phosphorus dynamics in pot experiments with different soil types, *Communications in Soil Science and Plant Analysis*, 33 (15-18) (2002) 3045-3058.
- [22] W.F. Maddams, The scope and limitations of curve fitting. *Applied Spectroscopy*, 34(3) (1980) 245-267.
- [23] M. Miyamoto, T. Arai, M. Komatsu, A. Yamamoto, T. Mikouchi, Evaluation of a curve-fitting method for diffuse reflectance spectra in the UV-Visible-NIR wavelength region, *Polar Science*, 3(2) (2009) 110-116.

- [24] A.J. Brown, Spectral curve fitting for automatic hyperspectral data analysis, *IEEE Transactions on Geoscience and Remote Sensing*, 44(6) (2006) 1601-1608.
- [25] J.M. Schmitt, G. Kumar, Spectral distortions in near-infrared spectroscopy of turbid materials, *Applied Spectroscopy*, 50(8) (1996) 1066-1073.
- [26] A.M. Mouazen, W. Saeys, J. Xing, J. De Baerdemaeker, H. Ramon, 2005, Near infrared spectroscopy for agricultural materials: an instrument comparison, *Journal of Near Infrared Spectroscopy*, 13 (2) 87-97.
- [27] M. Knadel, R.A. Viscarra Rossel, F. Deng, A. Thomsen, M. Humlekrog Greve, Visible–Near Infrared spectra as a proxy for topsoil texture and glacial boundaries, *Soil Science Society of America Journal*, 77(2) (2013) 568-579.
- [28] L.P. Marakkala Manage, M.H. Greve, M. Knadel, P. Moldrup, L.W. de Jonge, S. Katuwal, Visible-Near-Infrared spectroscopy prediction of soil characteristics as affected by soil-water content, *Soil science society of America Journal*, 82(6) (2018) 1333-1346.
- [29] E. Ben-Dor, Y. Inbar, Y. Chen, The reflectance spectra of organic matter in the visible near-Infrared and short wave infrared region (400-2500 nm) during a controlled decomposition process, *Remote Sensing of Environment*, 61(1) (1997) 1-15.
- [30] A.M. Mouazen, R. Karoui, J. De Baerdemaeker, H. Ramon, Characterization of soil water content using measured visible and near infrared spectra, *Soil Science Society of America Journal*, 70 (4) (2006) 1295-1302.
- [31] A.M. Mouazen, B. Kuang, J.D. Baerdemaeker, H. Ramon, Comparison among principal component, partial least squares and back propagation neural network analyses for accuracy of measurement of selected soil properties with visible and near infrared spectroscopy, *Geoderma*, 158 (1-2) (2010) 23-31.
- [32] T.I. McLaren, R.J. Smernik, M.J. McLaughlin, A.L. Doolette, A.E. Richardson, E. Frossard, The chemical nature of soil organic phosphorus: A critical review and global compilation of quantitative data, *Advances in Agronomy*, 160 (1) (2020) 51-124.
- [33] M.R. Maleki, L. Van Holm, H. Ramon, R. Merckx, J. De Baerdemaeker, A.M. Mouazen, Phosphorus sensing for fresh soils using visible and near infrared spectroscopy, *Biosystems Engineering*, 95(3) (2006) 425-436.
- [34] A. M. Mouazen, M. R. Maleki, J. De Baerdemaeker, H. Ramon, On-line measurement of some selected soil properties using a VIS-NIR sensor. *Soil & Tillage Research*, 93 (1) (2007) 13-27.

- [35] A.M. Mouazen, B.Y. Kuang, On-line visible and near infrared spectroscopy for in-field phosphorous management, *Soil & Tillage Research*, 155 (2016) 471-477.
- [36] M.R. Maleki, A.M. Mouazen, B. De Keterlaere; H. Ramon, J. De Baerdemaeker, On-the-go variable-rate phosphorus fertilisation based on a visible and near infrared soil sensor, *Biosystems Engineering*, 99(1) (2008) 35-46.